Spin transport of electrons through quantum wires with a spatially modulated Rashba spin-orbit interaction

X. F. Wang*
Department of Physics, Concordia University, 1455 de Maisonneuve Ouest, Montréal, Québec, Canada H3G 1M8
(Received 10 June 2003; revised manuscript received 25 August 2003; published 6 January 2004)

We study ballistic transport of spin-polarized electrons through quantum wires in which the Rashba spin-orbit interaction (SOI) is spatially modulated. Subband mixing, due to SOI, between the two lowest subbands is taken into account. Simplified approximate expressions for the transmission are obtained for electron energies close to the bottom of the first subband and near the value for which anticrossing of the two lowest subbands occurs. In structures with periodically varied SOI strength, *square-wave* modulation on the spin transmission is found when only one subband is occupied and its possible application to the spin transistor is discussed. When two subbands are occupied the transmission is strongly affected by the existence of SOI interfaces as well as by the subband mixing.

DOI: 10.1103/PhysRevB.69.035302 PACS number(s): 73.23.Ad, 72.25.Mk, 72.25.Dc

I. INTRODUCTION

With the development of nanotechnology, manipulation and measurement of spin-orbit interaction (SOI) in semiconductor nanostructures[1–7] have been realized as well as injection and detection of spin-polarized current.[8–17] As a result, in the past years increasing attention has been drawn to the spin-related behavior of quasi-one-dimensional (Q1D) electron systems in the presence of SOI, especially the Rashba SOI term, of strength α, which results from asymmetric electric confinement in nanostructures.[18] This has been also greatly stimulated by the proposal[19] of establishing a spin transistor, among other spintronic devices, and its potential application to the promising quantum computing. The SOI theory developed earlier for bulk materials[18] and two-dimensional electron systems[20] has been applied to the electronic band structure and spectral properties of realistic quantum wires.[24,21–23] Intriguing transport properties through quantum wires have been predicted as a result of peculiar features in their band structures introduced by the SOI, such as additional subband extrema and anticrossings. It has been found that the spatial distribution of the spin orientation in quantum wires can be greatly influenced by the subband mixing and the existence of interfaces between different SOI strengths.[23] Furthermore, the Rashba SOI has interesting effects on the shot noise for spin-polarized and entangled electrons,[25] and on the spectral properties of interacting quantum wires.[24] The former may lead to another way of measuring the SOI strength in quantum wires.

To run a spin transistor based on the SOI in a Q1D system, a spin filter is required to provide the initial spin-polarized current. One of the realistic options is to inject a spin current from ferromagnetic semiconductors or metals.[8–17] The spin-polarization of the injected current is independent of the existence of the SOI in the Q1D system[26] and this makes it possible to separate the study of the spin transistor from that of the spin filter. Recently, several efforts have been made to describe in more detail the behavior of spin polarized electrons in Q1D systems in the presence of the Rashba SOI. A numerical tight-binding simulation has been carried out to study ballistic transport[27] through a quantum wire in which one SOI segment is adiabatically connected to two segments without SOI. The results illustrate that a uniform spin precession along the wire should be observed provided the Rashba SOI strength is weak and subband mixing is negligible. For strong SOI, however, spin modulation becomes energy dependent and can be strongly suppressed at finite temperatures. Lately, a square-wave modulation of spin polarization and a good spin transistor behavior have been predicted in transport through periodically stubbed waveguides for weak SOI and subband mixing due to it occurring only in the stubs.[28] Although, in general, subband mixing results in disagreeable effects on spin precession in quantum wires, it can offer further control of spin polarization at low temperatures in some situations.[27–30]

In this paper we study ballistic transport of Q1D spin-polarized electron gases in the presence of a spatially modulated Rashba SOI strength α and taken into account the subband mixing between the first and second subbands. This modulation can be achieved experimentally by external gates[3] and may result in further modulation of spin currents, as pointed out in Refs. 27 and 23, and reported in Ref. 31 when subband mixing is neglected. Different from the periodically stubbed waveguides, with the same strength α everywhere, studied previously,[28,29] here we consider waveguides without stubs but with spatially modulated α, which, from an experimental point of view, are easier to realize and control. We assume that the electric confinement, that gives rise to the SOI, is strong enough that excited states due to this confinement, as observed in Ref. 7, are not occupied.

The paper is organized in the following way. In Sec. II we propose a model Hamiltonian with the Rashba SOI term to obtain the band structure and wave function. In Sec. III we formulate the transfer-matrix description of the transmission process and in Sec. IV we present and discuss the results of spin transport. Conclusions follow in Sec. V.

II. MODEL

We consider a Q1D electron system, an InGaAs/InAlAs quantum wire fabricated by confining a two-dimensional

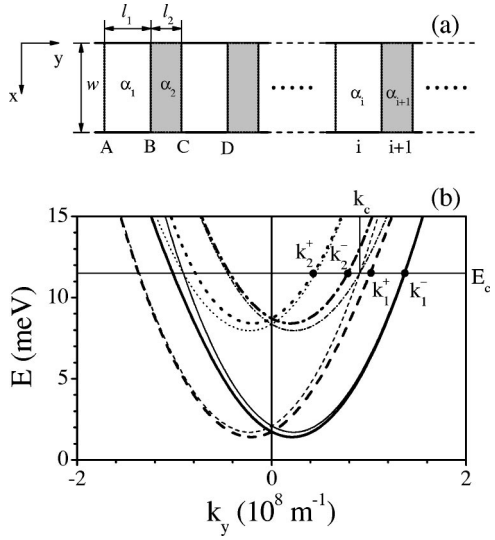

FIG. 1. (a) A quantum wire along the *y* direction composed of a series of segments $i=1,2,3,\ldots$ of SOI strength α_i and length l_i. (b) Energy dispersion of the lowest two subbands in a InGaAs quantum wire 600 Å wide. The thick (thin) solid, dashed, dotted, dash-dotted curves present branches ε_1^- (E_1^-), ε_1^+ (E_1^+), ε_2^- (E_2^-), and ε_2^+ (E_2^+) respectively.

(2D) electron system in the *x*-*y* plane by an infinitely high, square-well potential $V(x)$. The wire has width *w* along the *x* direction, as shown in Fig. 1(a). In the presence of the Rashba SOI the Q1D one-electron Hamiltonian reads

$$\hat{H}=-\lambda\nabla^2-i\alpha(\boldsymbol{\sigma}\times\nabla)_z+V(x), \tag{1}$$

where $\lambda=\hbar^2/2m^*$. $\nabla=(\partial/\partial x,\partial/\partial y,0)$ is the Laplace operator, α is the strength of the SOI, and $\sigma=(\sigma_x,\sigma_y,\sigma_z)$ denotes the spin Pauli matrices. In the σ_z representation and with the use of the eigenfunction of the Q1D Hamiltonian $h(x)=-\lambda\nabla_x^2+V(x)$ without the Rashba term, the eigenfunction is $\phi_m(x)=\sqrt{2/w}\sin(m\pi x/w)$ for $0\leqslant x\leqslant w$ and $m=1,2,3,\ldots$. Then the wave function of Eq. (1) can be expressed as $\Psi(k,\mathbf{r})=e^{iky}\Sigma_{m\sigma}\phi_m(x)C_m^\sigma|\sigma\rangle$ with $|\sigma\rangle=(1,0)^T$ for spin up and $(0,1)^T$ for spin down, with $\mathcal{X}^T$ denoting the transpose of the column matrix $\mathcal{X}$.

For the sake of simplicity, while retaining the subband mixing effects, we assume that only the lowest two subbands ($m=1$ and 2) are involved in the transport. This can be considered as the actual case when the temperature and the electron density are not too high. Then the secular equation $\hat{H}\Psi=E\Psi$ takes the form

$$\begin{bmatrix} E_1-E & \alpha k & 0 & -\delta \\ \alpha k & E_1-E & \delta & 0 \\ 0 & \delta & E_2-E & \alpha k \\ -\delta & 0 & \alpha k & E_2-E \end{bmatrix}\begin{pmatrix} C_1^+ \\ C_1^- \\ C_2^+ \\ C_2^- \end{pmatrix}=0, \tag{2}$$

where $E_m=E_m^0+\lambda k^2$ and E_m^0 is the *m*th subband bottom in the absence of SOI; $\delta=\alpha\int dx\,\phi_2(x)\phi_1'(x)=8\alpha/3w$ is the mixing term due to SOI between the first and the second subband. The resulting eigenvalues $\varepsilon_n^\sigma(k)$ and eigenvectors $\Psi_n^\sigma(k)$ are

$$\begin{cases} \varepsilon_1^\pm(k)=(E_1+E_2-\Delta E_\mp)/2, & \Psi_1^\pm(k)=\dfrac{1}{F_{\pm k}}\begin{pmatrix} \phi_1\mp 2\delta\phi_2/B_{\pm k} \\ \pm\phi_1+2\delta\phi_2/B_{\pm k}\end{pmatrix} \\ \varepsilon_2^\pm(k)=(E_1+E_2+\Delta E_\pm)/2, & \Psi_2^\pm(k)=\dfrac{1}{F_{\mp k}}\begin{pmatrix} \phi_2\mp 2\delta\phi_1/B_{\mp k} \\ \pm\phi_2+2\delta\phi_1/B_{\mp k}\end{pmatrix}. \end{cases} \tag{3}$$

Here $\Delta E_\pm=[(\Delta E_{12}\pm 2\alpha k)^2+4\delta^2]^{1/2}$, $\Delta E_{12}=E_2^0-E_1^0$, $B_{\pm k}=\Delta E_{12}\mp 2\alpha k+\Delta E_-$, and $F_{\pm k}=[2+8\delta^2/B_{\pm k}^2]^{1/2}$. Setting $\delta=0$ in Eq. (2) gives the eigenfunctions without subband mixing $|n,\pm\rangle=\phi_n(1,\pm 1)^T/\sqrt{2}$ with corresponding energy $E_n^\pm=E_n\pm\alpha k$. The resulting wave vector difference between the two spin branches of each subband for the same energy $E=E_n^+(k^+)=E_n^-(k^-)$, which we denote as the intrasubband SOI splitting, is constant for any energy and has the value

$$k_\alpha=k^--k^+=2m^*\alpha/\hbar^2. \tag{4}$$

In Fig. 1(b) we plot the energy spectrum of the lowest two subbands with (thick curves) and without (thin curves) the mixing term taken into account. This energy spectrum is essentially the same as that shown in Fig. 2 of Refs. 29 and 30. The intersections of the Fermi energy, here taken equal to the anticrossing energy E_c as shown by the horizontal bar, with the energy spectrum define the wave vectors of the propagating modes. E_c is given by $E_c=E_1^+(k_c)=E_2^-(k_c)=5E_1/2+9\hbar^2E_1^2/(8m^*\alpha^2)$, where the branches without mixing E_1^+ and E_2^- (E_1^- and E_2^+) anticross each other at the wave vectors k_c ($-k_c$). Without mixing, the Fermi wave vector difference between the two spin branches of each subband remains constant. With mixing, however, the difference between ε_n^- and ε_n^+ branches shows an energy dependence. Furthermore, in the branches $E_n^\pm$ electrons have the same spin orientation, but in the branches $\varepsilon_n^\pm$, which are not pure spin states, the average electronic spins rotate continuously from their low-energy orientation to their opposite high-energy orientation, as also discussed recently in Ref. 23. At the anticrossing energy, the maximum mixing effect happens between forward propagating electrons in the ε_1^+ and ε_2^- branches [corresponding to $B_k=2\delta$ in Eq. (3)] and between backward ones in the ε_1^- and ε_2^+ branches ($B_{-k}=2\delta$). We denote the wave-vector difference between the $\varepsilon_1^\pm$ and $\varepsilon_2^\mp$

branches at this energy as the intersubband SOI splitting $2k_\delta$ related to k_c. For $\alpha<2\hbar^2/m^*w$, we have

$$k_\delta \approx \frac{m^*\delta}{\hbar^2 k_c}=\frac{8k_\alpha^2}{9\pi^2}w. \tag{5}$$

III. TRANSFER MATRIX

We consider a quantum wire with a variable strength of SOI. It may be composed of a series of SOI segments separated by SOI interfaces. In each SOI segment, the SOI strength is approximately uniform and the Hamiltonian described in the preceding section applies. To describe the electronic behavior propagating through the quantum wire, we begin considering the transmission process of an electron with energy E through one SOI interface. The electron is incident from the left to the interface joining two segments (labeled i and $i+1$) with different SOI strength α_i and α_{i+1} as shown in Fig. 1(a). Taking into account only the lowest two subbands, we write the wave function in segment i, in terms of of the eigenfunction $\Psi_{ni}^{\pm}$ given by Eq. (3) as

$$\varphi_i(x,y)=\sum_{\pm}\left[c_{1i}^{\pm}\Psi_{1i}^{\pm}(k_{1i}^{\pm})e^{ik_{1i}^{\pm}y}+\overline{c_{1i}^{\pm}}\Psi_{1i}^{\pm}(-k_{1i}^{\mp})e^{-ik_{1i}^{\mp}y}\right.$$
$$\left.+c_{2i}^{\pm}\Psi_{2i}^{\pm}(k_{2i}^{\pm})e^{ik_{2i}^{\pm}y}+\overline{c_{2i}^{\pm}}\Psi_{2i}^{\pm}(-k_{2i}^{\mp})e^{-ik_{2i}^{\mp}y}\right]. \tag{6}$$

To obtain proceed we follow the approach of Ref. 26: we match the wave function and its flux at the interfaces between the i and $i+1$ segments. The velocity operator is given by

$$\hat{v}_y=\frac{\partial H}{\partial p_y}=\begin{bmatrix} -i\dfrac{\hbar}{m^*}\dfrac{\partial}{\partial y} & \dfrac{\alpha}{\hbar} \\ \dfrac{\alpha}{\hbar} & -i\dfrac{\hbar}{m^*}\dfrac{\partial}{\partial y}\end{bmatrix}. \tag{7}$$

The continuity of the wave function at the interface $y=y_{i,i+1}$, between the i and $i+1$ segments, gives $\varphi_i(x,y_{i,i+1})=\varphi_{i+1}(x,y_{i,i+1})$ and that of the flux $\hat{v}_y\varphi_i(x,y)|_{y_{i,i+1}}=\hat{v}_y\varphi_{i+1}(x,y)|_{y_{i,i+1}}$. Multiplying the two equations by $\Psi_{1i}^{*\pm}(k)$ and $\Psi_{2i}^{*\pm}(k)$, respectively, then integrating over x we obtain eight linear equations for the eight coefficients of the wave functions. Here we drop the subscript and superscript pertaining to k since they are the same as those for Ψ as shown in Eq. (6). Because electrons in branches Ψ_{1i}^{+} and Ψ_{2i}^{-} are decoupled from electrons in branches Ψ_{1i}^{-} and Ψ_{2i}^{+}, a result of the symmetric property of the wave function, these equations are grouped into two similar but independent equation groups with each composed of four equations. The group corresponding to modes Ψ_{1i}^{+} and Ψ_{2i}^{-} connects the column matrix $\hat{R}_i=(c_{1i}^{+},\overline{c_{1i}^{+}},c_{2i}^{-},\overline{c_{2i}^{-}})^T$ and column matrix $\hat{L}_{i+1}=(c_{1i+1}^{+},\overline{c_{1i+1}^{+}},c_{2i+1}^{-},\overline{c_{2i+1}^{-}})^T$ and reads:

$$\hat{S}_i\hat{R}_i=\hat{Q}_{i+1}\hat{L}_{i+1}. \tag{8}$$

Denoting the scalar product $\langle\Psi|\Psi'\rangle$ in all matrix products by the integral $\int\Psi^{*T}(x,y)\Psi'(x,y)dx$ and the direct product of the column matrix $\mathcal{X}$ with the row matrix $\mathcal{Y}$ by $\mathcal{X}\otimes\mathcal{Y}$, the upper (2×4) part of the 4×4 matrix $\hat{S}_i$ is given by $\mathcal{A}_i\otimes\mathcal{B}_i$ and the lower part by $\mathcal{A}_i\otimes\mathcal{C}_i$, while the upper (2×4) part of the 4×4 matrix $\hat{Q}_{i+1}$ is given by $\mathcal{A}_i\otimes\mathcal{B}_{i+1}$ and the lower part by $\mathcal{A}_i\otimes\mathcal{C}_{i+1}$. Here $\mathcal{A}_i=[\langle\Psi_{1i}^{+}(k)|,\langle\Psi_{2i}^{-}(k)|]^T$, $\mathcal{B}_i=[|\Psi_{1i}^{+}(k)\rangle,|\Psi_{1i}^{+}(-k)\rangle,|\Psi_{2i}^{-}(k)\rangle,|\Psi_{2i}^{-}(-k)\rangle]$ and $\mathcal{C}_i=[|\xi_{1i}^{+}(k)\rangle,|\xi_{1i}^{+}(-k)\rangle,|\xi_{2i}^{-}(k)\rangle,|\xi_{2i}^{-}(-k)\rangle]$ with $|\xi\rangle=\hat{v}_y|\Psi\rangle$.

If the SOI exists only in segment $i+1$ ($\alpha_i=0$ and $\alpha_{i+1}=\alpha$), we discard all the subscripts $i+1$ in the matrices $\hat{S}_i$ and $\hat{Q}_{i+1}$ and explicitly express them as

$$\hat{S}_i=\begin{bmatrix} 1 & 1 & 0 & 0 \\ 0 & 0 & 1 & 1 \\ k_1^0/m^* & -k_1^0/m^* & 0 & 0 \\ 0 & 0 & k_2^0/m^* & -k_2^0/m^*\end{bmatrix} \tag{9}$$

and

$$\hat{Q}_{i+1}=\sqrt{2}\begin{bmatrix} \dfrac{1}{\Theta_1} & \dfrac{1}{\overline{\Theta}_1} & \dfrac{2\delta}{\Theta_2\Lambda_2} & \dfrac{2\delta}{\overline{\Theta}_2\overline{\Lambda}_2} \\ -\dfrac{2\delta}{\Theta_1\Lambda_1} & -\dfrac{2\delta}{\overline{\Theta}_1\overline{\Lambda}_1} & \dfrac{1}{\Theta_1} & \dfrac{1}{\overline{\Theta}_2} \\ \dfrac{1}{\Theta_1}\left(\dfrac{\alpha}{\hbar^2}+\dfrac{k_1^+}{m^*}\right) & \dfrac{1}{\overline{\Theta}_1}\left(\dfrac{\alpha}{\hbar^2}-\dfrac{k_1^-}{m^*}\right) & \dfrac{2\delta}{\Theta_2\Lambda_2}\left(\dfrac{\alpha}{\hbar^2}+\dfrac{k_2^-}{m^*}\right) & \dfrac{2\delta}{\overline{\Theta}_2\overline{\Lambda}_2}\left(\dfrac{\alpha}{\hbar^2}-\dfrac{k_2^+}{m^*}\right) \\ \dfrac{2\delta}{\Theta_1\Lambda_1}\left(\dfrac{\alpha}{\hbar^2}-\dfrac{k_1^+}{m^*}\right) & \dfrac{2\delta}{\overline{\Theta}_1\overline{\Lambda}_1}\left(\dfrac{\alpha}{\hbar^2}+\dfrac{k_1^-}{m^*}\right) & \dfrac{1}{\Theta_2}\left(\dfrac{\alpha}{\hbar^2}-\dfrac{k_2^-}{m^*}\right) & \dfrac{1}{\overline{\Theta}_2}\left(\dfrac{\alpha}{\hbar^2}+\dfrac{k_2^+}{m^*}\right)\end{bmatrix}. \tag{10}$$

Here $k_1^0=[2m^*(E-E_1^0)]^{1/2}/\hbar$ ($k_2^0=[2m^*(E-E_2^0)]^{1/2}/\hbar$) is the wave vector of the electrons in the first (second) subband in the segment without SOI and $\Lambda_1=B_{k_1^+}$, $\overline{\Lambda}_1=B_{-k_1^+}$, $\Lambda_2=B_{k_2^-}$, $\overline{\Lambda}_2=B_{-k_2^-}$, $\Theta_1=F_{k_1^+}$, $\overline{\Theta}_1=F_{-k_1^+}$, $\Theta_2=F_{k_2^-}$, and $\overline{\Theta}_2=F_{-k_2^-}$ are defined in the segment with SOI of strength α.

The above complex matrix can be simplified approximately in the low-energy limit ($E\gtrsim E_1^0$) and the anticrossing energy limit ($E\approx E_c$). If the electron density is sufficiently low that the Fermi energy is close to the bottom of the first subband E_1^0 in segment i, the correction to the wave function caused by subband mixing is negligible or we have $\Theta=\overline{\Theta}=\sqrt{2}$ and $\delta=0$ in Eqs. (9) and (10). We find all the spin modes in the quantum wire are decoupled from each other and the transfer equations for all modes have similar forms. The transfer equation for the mode Ψ_1^+ has the form

$$\begin{bmatrix} 1 & 1 \\ k_1^0 & -k_1^0 \end{bmatrix}\begin{pmatrix} c_{1i}^+ \\ \overline{c_{1i}^+} \end{pmatrix}=\begin{bmatrix} 1 & 1 \\ K_2 & -K_2 \end{bmatrix}\begin{pmatrix} c_{1i+1}^+ \\ \overline{c_{1i+1}^+} \end{pmatrix}, \tag{11}$$

with $K_2=(1/\hbar)[2m^*(E-E_1^0+\varepsilon_0+V_0)+(m^*\alpha/\hbar)^2]^{1/2}$ and $\varepsilon_0\approx\delta^2/\Delta E_{12}$ the energy correction to the first subband as a result of the SOI subband mixing. V_0 denotes the conduction-band offset in the segment $i+1$ reckoned from the conduction-band bottom in segment i, which may be introduced by material mismatch at the interface or by an external gate bias.

When the SOI strength is in the range $\hbar^2/m^*w<\alpha<2\hbar^2/m^*w$, the anticrossing energy is higher then the second subband bottom but lower than the third subband bottom and the intersubband SOI splitting is much smaller than the intrasubband SOI splitting, i.e., $k_\delta\ll k_\alpha$. Equation (9) and (10) can be greatly simplified if the electron energy is near to the anticrossing energy, i.e., $E\simeq E_c$. In this case, we use the approximation $V_0=0$, $\Lambda_1\approx 2\delta\sqrt{k_2^-/k_1^+}$, $\Lambda_2\approx 2\delta\sqrt{k_1^+/k_2^-}$, $\overline{\Lambda}_1\approx 8\alpha k_1^0$, $\overline{\Lambda}_2\approx 8\alpha k_2^0$, $\Theta_1\approx 2\sqrt{k_1^+/k_1^0}$, $\Theta_2\approx 2\sqrt{k_2^+/k_2^0}$, $\overline{\Theta}_1\approx\overline{\Theta}_2\approx\sqrt{2}$, $k_1^+\approx k_c+k_\delta$, $k_2^-\approx k_c-k_\delta$, $k_1^-\approx k_c+k_\alpha$, $k_2^+\approx k_c-k_\alpha$, $k_1^0\approx k_c+k_\alpha/2$, $k_2^0\approx k_c-k_\alpha/2$, $\delta/\overline{\Lambda}\approx 0$. Equation (8) reduces to

$$\begin{pmatrix} c_{1i}^+ \\ \overline{c_{1i}^+} \\ c_{2i}^- \\ \overline{c_{2i}^-} \end{pmatrix}=\begin{bmatrix} \sqrt{k_1^+/2k_1^0} & 0 & \sqrt{k_2^-/2k_1^0} & 0 \\ 0 & 1 & 0 & 0 \\ -\sqrt{k_1^+/2k_2^0} & 0 & \sqrt{k_2^-/2k_2^0} & 0 \\ 0 & 0 & 0 & 1 \end{bmatrix}\begin{pmatrix} c_{1i+1}^+ \\ \overline{c_{1i+1}^+} \\ c_{2i+1}^- \\ \overline{c_{2i+1}^-} \end{pmatrix}. \tag{12}$$

We see that, in the anticrossing energy limit, the mixing happens mainly between the two modes involved in the anticrossing (c_1^+ and c_2^-) and the modes corresponding to the coefficients $\overline{c_1^+}$ and $\overline{c_2^-}$ remain almost intact when transmitting from segment i to segment $i+1$ though there is a wave vector mismatch between the two segments.

Once the matrices $\hat{S}_i^{-1}$ and $\hat{Q}_{i+1}$ in Eq. (8) are known, the transfer matrix for the interface joining segment i and $i+1$ is obtained simply, $M_{i,i+1}=\hat{S}_i^{-1}\hat{Q}_{i+1}$. For a quantum wire with n segments, the total transfer matrix then reads

$$\hat{M}=\hat{P}_1\prod_{i=1,n-1}\hat{M}_{i,i+1}\hat{P}_{i+1}, \tag{13}$$

where the transfer matrix for the ith segment of length l is expressed as

$$\hat{P}_i=\begin{bmatrix} e^{-ik_{1i}^+l} & 0 & 0 & 0 \\ 0 & e^{ik_{1i}^-l} & 0 & 0 \\ 0 & 0 & e^{ik_{2i}^-l} & 0 \\ 0 & 0 & 0 & e^{-ik_{2i}^+l} \end{bmatrix}. \tag{14}$$

A transfer matrix similar to $\hat{M}$ given by Eq. (13) is obtained for the modes Ψ_{1i}^- and Ψ_{2i}^+ by applying the same process as above and will not be shown here. Finally a 8×8 transfer matrix $\hat{T}$ is obtained connecting the wave-function coefficients of the electron with energy E at the left inlet end, $\hat{I}=(c_{1I}^\pm,\overline{c_{1I}^\pm},c_{2I}^\pm,\overline{c_{2I}^\pm})^T$, and at the right outlet end, $\hat{O}=(c_{1O}^\pm,\overline{c_{1O}^\pm},c_{2O}^\pm,\overline{c_{2O}^\pm})^T$, in the form $\hat{I}=\hat{T}\hat{O}$.

IV. RESULTS AND DISCUSSION

In the following we present results for ballistic transport of electrons, incident with spin up (along the z direction), through a quantum wire in which segments with and without SOI alternate periodically. If not otherwise specified, zero temperature and parameters $w=600$ Å, $l=2500$ Å, $\alpha=3.45\times 10^{-11}$ eVm, $m^*=0.05$, and $V_0=0$ will be assumed. The strength of SOI can be adjusted experimentally[3–6] and here we use the same value of α as used in Ref. 30 for the sake of comparison. At zero temperature, only electrons of the Fermi energy contribute to the transport. In the inlet and outlet segments of the quantum wire, we assume that there is no SOI and the group velocity of the electrons is proportional to the wave vector ($k_n^0=[2m^*(E-E_n^0)]^{1/2}/\hbar$, $n=1,2$) and the density of states to its inverse. When using the normalized coefficients for the input wave function ($c_{1I}^\pm=1/\sqrt{2k_1^0}, c_{2I}^\pm=1/\sqrt{2k_2^0}$), we express the zero-temperature spin-up (spin-down) partial conductance $G_n^+(G_n^-)$ and the partial transmission $T_n^+(T_n^-)$ at the outlet end via the subband n and the reflection R_n^+ (R_n^-) from the inlet end as

$$G_n^\pm=\frac{e^2}{h}T_n^\pm=\frac{e^2}{h}\frac{k_n}{2}|c_{nO}^+\pm c_{nO}^-|^2,\quad R_n^\pm=\frac{k_n}{2}|\overline{c_{nI}^+}\pm\overline{c_{nI}^-}|^2. \tag{15}$$

The finite-temperature conductance $G_n^\pm(T)$ is obtained by integrating over energy the above zero-temperature conductance multiplied by the Fermi distribution function f_n,

$$G_n^\pm(T)=-\int dE G_n^\pm(E,T=0)\frac{df_n(E,T)}{dE}. \tag{16}$$

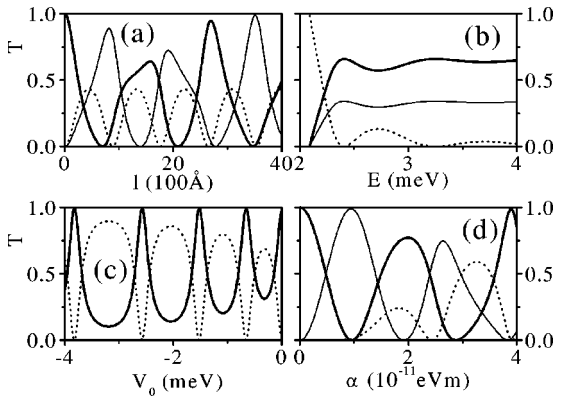

FIG. 2. Transmission T^+ (thick solid curves) and T^- (thin solid curves), and reflection R^+ (dotted curves) of a quantum wire with one SOI segment as a function of (a) l, (b) E, (c) V_0 of the SOI segment of length $l=2800$ Å, and (d) α when $E=\varepsilon_1(0)+0.1$ meV. The result in (a) and (c) corresponds to the electrons of energy $E=\varepsilon_1(0)+0.2$ meV with $\varepsilon_1(0)=2.09$ meV.

A. The low-energy limit

If only the first subband is occupied and E_c and E_2^0 are much above the Fermi energy, Eq. (11) can be used to estimate the transmission through the quantum wire. In a quantum wire with only one SOI segment, of strength $\alpha_2=\alpha$ and length $l_2=l$, sandwiched between two segments without SOI as the part *A*-*B*-*C*-*D* shown in Fig. 1(a), the total transmission takes the form

$$T=\frac{t}{t\cos^2(K_2 l)+\sin^2(K_2 l)}, \tag{17}$$

where $t=4(k_1^0)^2K_2^2/[(k_1^0)^2+K_2^2]^2$. This is a sinusoidal dependence with a maximum $T_{max}=1$ for $\sin(K_2 l)=0$ and a minimum $T_{min}=t$. For a quantum wire of fixed width, the stronger is the SOI strength and the less is the energy of the incident electrons, the more efficient is the modulation of the transmission. Another feature of this interface-induced transmission modulation is that it does not affect the spin polarization. The output percentage of spin-up and spin-down electrons remains the same as predicted neglecting the interface effect, $T^+=T\cos^2(\theta/2)$ and $T^-=T\sin^2(\theta/2)$ with $\theta=k_\alpha l$. These features offer the possibility of independent control of the total transmission and of the spin polarization and will be advantageous when designing a spin transistor employing this system.

In Fig. 2, we plot T^+ (thick solid curves), T^- (thin solid), and R^+ (dotted) as a function of the main parameters of the quantum wire. Since only spin-up electrons are incident and there is no spin-flip mechanism, spin-down reflection is not observed. The spin-up and spin-down electrons output flux show, in Fig. 2(a), a modulated sinusoidal dependence on the length l of the SOI segment instead of the simple one as the interface effect is neglected.[19] For electrons near the bottom of the first subband, a strongly energy-dependent reflection happens [Fig. 1(b)] due to the wave-vector mismatch between electrons in segments with and without SOI. A similar energy dependence of the conductance (transmission) has also been found in Ref. 27. In some cases, e.g., when an extra gate bias is applied, an offset V_0 exists between the conduction bands of the material in the segment with SOI and the one without SOI and can be adjusted. This may introduce further modulation to the spin transmission. Figure 2(c) illustrates the oscillatory dependence of the transmission and the reflection on this offset. An increasing amplitude of the oscillation is found for a lower conduction-band bottom of the SOI segment. Here $l=2800$ Å is chosen so that no spin-down transmission is observed. An oscillatory dependence of the transmission and reflection is also found as a function of the SOI strength as shown in Fig. 2(d). For $\alpha>1.5\times10^{-11}$ eVm the reflection of low-energy electrons may become significant.

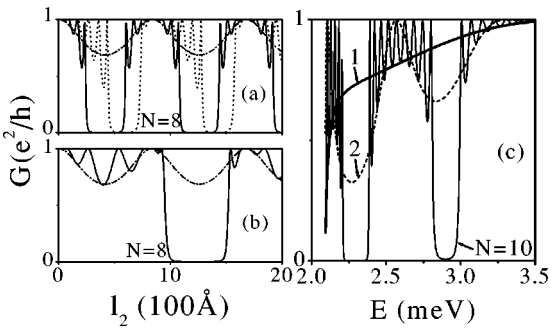

FIG. 3. (a) Total conductance of a periodic structure of 8 identical units as functions of the length l_2 of the SOI segment when fixing the length l_1 of the segment without SOI at $l_1=2375$ Å (solid curve) and $l_1=2000$ Å (dotted curve). (b) The same as (a) when the total length of each unit is fixed to $l_1+l_2=2100$ Å. The dash-dotted curves in (a) and (b) are results for one-unit cases. (c) Conductance in a periodic structure of N identical units as functions of the electron energy when $l_1=1350$ Å and $l_2=1100$ Å. The numbers beside the curves label N.

Now we introduce a periodic structure consisting of identical units that are repeated along the wire. Each unit is composed of one non-SOI segment of length l_1 and one SOI segment of strength α and length l_2 as shown in Fig. 1(a). Electrons are incident at the left end and exiting at the other; both ends are segments without SOI. Because the Fabry-Perot-like interference of electron waves happens between interfaces connecting regions with different SOI strengths and then different energy-momentum dispersion relations, the transmission minima of one SOI segment described by Eq. (17) deepen with the increase of the number of units and transform into transmission gaps when the number is big enough. This happens in a similar way as in the Krong-Penney model of solids. As shown in Fig. 3(a), where each curve corresponds to a fixed l_1, almost square wave curves (solid and dotted curves) as functions of l_2 are observed in structures of eight units, comparing with the sinusoidal total transmission T (dash-dotted curves) for one unit. For structures with more units, increased frequency and amplitude of the oscillations between the gaps are observed. The position and width of the conductance gaps shift when varying l_1. If we fix the total length l_1+l_2 of each unit, similar square-wave transmission is obtained as shown in Fig. 3(b) but with different gap width. The percentage of the spin-up and spin-

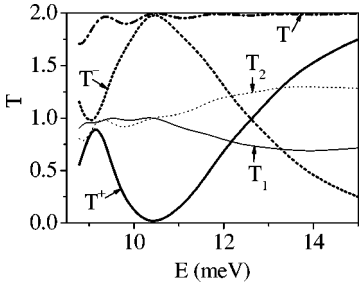

FIG. 4. Transmission vs electron energy when two subbands are occupied in a quantum wire with one SOI segment of length $l = 2000$ Å. The total transmission T (dash-dotted curve) and partial transmissions corresponding to different spin orientations $T^{\pm}$ (thick solid for $+$ and thick dotted for $-$) and different subbands T_n (thin solid and dotted for $n=1$ and 2, respectively) are shown separately. The bottom of the second subband in the SOI segment is about 8.8 meV.

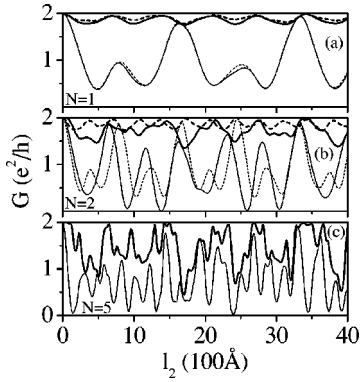

FIG. 5. The total (thick curves) and the spin-up (thin curves) conductance are illustrated as functions of the SOI-segment's length l_2 for electrons incident with energy $E=9$ meV. The solid curves in (a), (b) , and (c) are the results for a structure of 1, 2, and 5 SOI segments, respectively, with $l_1=1250$ Å. The dotted curves in (b) constitute the two-segment result with $l_1=1000$ Å. The dotted curves in (a) is the double of the conductance obtained by assuming electrons are incident from only the first subband.

down conductances here depends only on the total length of the SOI segment and k_α and can be easily figured out in the same way as that for one-unit quantum wires.

A similar square-wave conductance can also be found as a function of the electron energy. For a quantum wire with only one SOI segment, the transmission increases monotonically as a function of the energy and approaches unity when the electron wave vector is much larger than k_α as shown by the thick curve in Fig. 3(c). A simple oscillating conductance (the dotted curve) appears in a quantum wire with two SOI segments; square conductance gap can be observed in a wire with ten (thin solid curve) or more units and miniband develops in a SOI superlattice as appears generally in periodic structures.

B. Two-subband transmission

Electrons can propagate via the second subband when their energy is high enough. In the trivial case of weak SOI strength that subband mixing is negligible, each mode propagates through the quantum wire almost independently, the spin transmission of electrons in the second subband can be estimated in a similar way as in the first subband by Eq. (11). Results similar to those obtained in the low-energy limit of the first subband are also obtained for the second subband and will not be shown here in detail. In the following we will concentrate on the SOI-interface effect on the two-subband transmission when the subband mixing is important.

In Fig. 4 we show the energy dependence of the total transmission T (dash-dotted curve), spin transmission $T^{\pm}$ (thick solid and dotted curves), and transmission from the first $T_1=T_1^+ + T_1^-$ and the second $T_2=T_2^+ + T_2^-$ subband (thin curves). The reflection becomes significant mainly for those electrons propagating via the second subband when the electron energy is close to the second subband bottom, $\varepsilon_2(0)$, and is not as strong as observed for electrons of energy near the first-subband bottom. At higher values of energy, the reflection becomes negligible and more electrons come out from the second subband. As a result of the subband mixing and corresponding energy-band modification, the percentage of spin-up and spin-down electrons is strongly dependent on the electron energy as also reported in Ref. 27. In quantum wires with multiple SOI segments, the transmission is further modulated for the same reason as discussed in the one subband case but the modulation is much more complex and irregular as a result of the coupling between different modes at interfaces.

In a Q1D electron system formed from an ideal 2D system, where the SOI strength is independent of the electron density as studied in this paper, the carrier density dependence of the ballistic conductance (transmission) can easily be figured out from their energy dependence plotted in Fig. 4. However, in a realistic semiconductor system[3] the SOI strength and the quantum wire width may vary as the carrier density changes. The density dependence of the conductance should be estimated using a more realistic model taking these effects into account. Another point concerning realistic systems is the effect of excited states due to the confinement along z direction, which introduces the SOI and forms a quasi-2D system rather than an ideal 2D system in the x-y plane. As observed in Ref. 7, the excited states of the quasi-2D system can be occupied when the carrier density is high. In a simple approximation, this case can be treated as a two-carrier system where the electrons in the ground state and the excited state transport independently if the confinement along x direction is symmetric. As a result, the conductance will be enhanced because more channels are opened to transport electrons.

In Fig. 5 we calculate the total conductance G (thick curves) and the spin-up conductance G^+ (thin curves) as functions of the SOI-segment length l_2 through periodic structures consisting of (a) $N=1$, (b) $N=2$, and (c) $N=5$ units for a Fermi energy $E_F=E=9$ meV close to the bottom of the second subband, where strong mismatch of the wave functions of the second subband is expected at the interfaces. For $N=1$ the transmission shows a periodic pattern and the reflection is limited. In contrast to the low-energy transmission discussed in the preceding subsection, the spin-up con-

ductance here does not vanish, i.e., the spin cannot be inverted completely by the structure, because the spin of electrons in the first-subband precesses with a frequency twice that in the second subband at this energy. Even if we assume that the electrons are incident only from the lowest subband, i.e., by letting $c_{2I}^{\pm}=0$ when carrying out the calculation, a similar result is obtained as shown by the thick and thin dotted curves (doubled) in Fig. 5(a). It is worthy of noting that the transmission estimation by assuming one-mode incidence as used in Ref. 30 is a good approximation for one-SOI-segment systems though not for multiple-SOI-segment ones. In the above structure if we put two identical SOI segments and separate them by a segment without SOI of length l_1, a similar pattern of the spin-up conductance as above appears but the oscillation frequency is almost doubled as shown in Fig. 5(b), where the results corresponding to $l_1=1250$ Å (solid curves) and $l_1=1000$ Å (dotted curves) are plotted. The segment without SOI can change the relative phase of electrons between interfaces and then the relative spin orientation between electrons in the first and second subbands, therefore, the initial spin-up electrons can be totally spin-flipped by the structure with $l_1=1250$ Å but not by that with $l_1=1000$ Å as the thin curves indicate in Fig. 5(b). With increasing number of SOI segments or SOI interfaces, the modulation of the conductance becomes complex and develops into conductance fluctuation. As an example, we plot the results for a five-SOI-segment structure in Fig. 5(c). The total conductance oscillates or fluctuates as a function of l_2 and the corresponding amplitude increases with increasing number of units. Strong reflection happens when the number of the units is large enough and the multi-SOI-segment structures can be used as electron filters even if two modes exist.

C. The anticrossing-energy limit

At the anticrossing energy E_c, opposite spin states from the first and second subbands mix strongly with each other. Nevertheless, simple transmission patterns can be found even in structures with multiple SOI segments. In a quantum wire with one-SOI segment of length $l_2=l$ sandwiched between two segments (ends) without SOI, the coefficient of the output wave function in the anticrossing-energy limit is obtained approximately with the help of Eqs. (12) and (13),

$$\begin{pmatrix} c_{1O}^{+} \\ c_{1O}^{-} \\ c_{2O}^{+} \\ c_{2O}^{-} \end{pmatrix} = e^{ik_c l} \begin{pmatrix} c_{1I}^{+}\cos(k_\delta l) - ic_{2I}^{-}\sqrt{k_2^0/k_1^0}\sin(k_\delta l) \\ c_{1I}^{-}\exp(ik_\alpha l) \\ c_{2I}^{+}\exp(-ik_\alpha l) \\ -ic_{1I}^{+}\sqrt{k_2^0/k_1^0}\sin(k_\delta l) + c_{2I}^{-}\cos(k_\delta l) \end{pmatrix}$$
$$= \frac{e^{ik_c l}}{\sqrt{2}} \begin{pmatrix} e^{-ik_\delta l}/\sqrt{k_1^0} \\ e^{ik_\alpha l}/\sqrt{k_1^0} \\ e^{-ik_\alpha l}/\sqrt{k_2^0} \\ e^{-ik_\delta l}/\sqrt{k_2^0} \end{pmatrix}. \quad (18)$$

Here the normalized coefficients ($c_{1I}^{\pm}=1/\sqrt{2k_1^0}, c_{2I}^{\pm}=1/\sqrt{2k_2^0}$) of the incident waves are used to get the right-hand side (rhs) of the above equation. The spin-up (spin-down) transmission then reads

$$T^{\pm}=1\pm\cos(k_\alpha l)\cos(k_\delta l) \quad (19)$$

with $T_1^{\pm}=1/2\pm 1/2\cos(k_\alpha+k_\delta)l$ the transmission out of the first subband and $T_2^{\pm}=1/2\pm 1/2\cos(k_\alpha-k_\delta)l$ out of the second subband. For a rational ratio of $k_\alpha/k_\delta \approx 9\pi^2\hbar^2/(16m^*\alpha w)$ the transmission is approximately a periodic function of the length of the SOI segment.

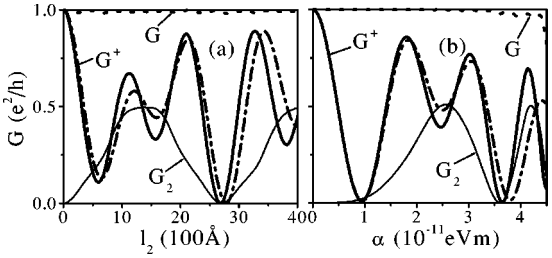

FIG. 6. The conductance is plotted as a function of the length of the SOI segment (a) and of the SOI strength α (b) when electrons of the anticrossing energy of the SOI segment are assumed incident from only the first subband. The thick solid, thin solid, and dotted curves present the spin-up, second-subband, and total conductances, respectively, obtained numerically. As a comparison, the dash-dotted curves show the spin-up conductance obtained from Eq. (19).

Assuming electrons are incident only from the first subband ($c_{2I}^{\pm}=0$), we get the same approximate transmission as Eq. (19) but divided by two. This result is also the same as that found in Ref. 30 where the interface effect is neglected. In Fig. 6(a) we show the conductance versus l and in Fig. 6(b) versus α. The Fermi energy of the electron gas is equal to the anticrossing energy $E_c(\alpha)$ and the electrons are assumed incident from only the first subband. The dash-dotted and the thick solid curves represent the spin-up conductance given, respectively, by the simplified expression Eq. (19) and by the numerical solution of Eqs. (8)–(10). When the anticrossing energy locates well between the minima of the second and the third subbands, corresponding to $2.5<\alpha<3.5\times10^{-11}$ eVm here, the total transmission, shown by the dotted curves, is almost unity and Eq. (19) can be used to estimate the spin transmission through a quantum wire with a SOI segment of length up to several thousands of angstroms. Nevertheless, when $k_\delta l\sim n\pi/2$ for odd number n almost half of the electrons transit from the first subband to the second subband (corresponding to $G_2\sim 0.5e^2/h$ shown by the thin solid curves in Fig. 6) and Eq. (19) is in poorer agreement with the numerical result. For a lower anticrossing energy or $\alpha>4\times10^{-11}$ eVm the reflection due to SOI interface becomes important and Eq. (19) becomes less reliable. For $\alpha<2.5\times10^{-11}$ eVm, the corresponding anticrossing energy is higher than the third subband and the result given in Fig. 6(b) should be corrected by considering the effect of the third subband.

Actually, electrons should be incident simultaneously from both the first and the second subbands if the quantum wire is connected to a Fermi electron reservoir with Fermi

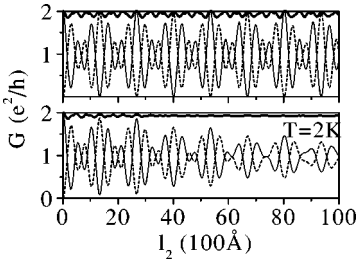

FIG. 7. Conductance through a two-SOI-segment quantum wire as a function of l_2 at zero temperature (upper plot) and at temperature $T=2$ K (lower plot). G (thick solid curves), G^+ (thin solid), and G^- (dotted) are shown. The parameters are chosen such that $k_\alpha l_2 = 4k_\delta l_2 = 4k_0 l_1 = 8\pi$ for $l_2 = 5352$ Å.

energy higher then the second-subbands bottom. At the anticrossing energy, the wave functions of the first and the second subband mix equally with each other and electrons propagate almost equally through each subband. The spin-up and total conductances have quite similar dependence on l_2 and α as those plotted in Fig. 6 with doubled values. In fact, even when the Fermi energy is far away from the anticrossing energy but in the second subband, the spin-up and spin-down conductances $G^\pm$ of a Fermi gas can be well estimated by doubling the one obtained by assuming incidence from one subband as illustrated in Fig. 5(a), where the Fermi energy is close to $\varepsilon_2(0)$. Comparing the conductance pattern in Fig. 5(a) with that in Fig. 6(a), we see mainly two different features. At first, the reflection of electrons at E_c is much lower because the mismatch of wave function is less. Second, both the spin-up and the spin-down conductances at E_c can vanish but only the spin-down one vanishes at energy near $\varepsilon_2(0)$. This is a result of the fact that the ratio between the precession frequencies of electrons in the first and the second subbands changes with the electron energy. The ratio is 5/3 in Fig. 6(a) comparing to 2 in Fig. 5(a).

In quantum wires with two SOI segments, the spin transmission at zero temperature is approximately expressed as

$$T^\pm \approx 1 \pm \cos k_0 l_1 \cos(2k_\delta l_2)\cos(k_0 l_1 + 2k_\alpha l_2) \pm \sin k_0 l_1 \sin(k_0 l_1 + 2k_\alpha l_2). \quad (20)$$

Here $k_0 = (k_1^0 - k_2^0)/2$, with k_1^0 and k_2^0 the wave vectors of the first and second subbands in the segment without SOI. The conductance as a function of l_2 shows a periodic pattern if the ratio k_α/k_δ is rational. In Fig. 7, we show the conductance as a function of the length of the SOI segment l_2 at zero-temperature (upper panel) and at temperature $T=2$ K (lower panel). We choose the wire width as $w=609$ Å so that $k_\alpha = 2k_0 = 4k_\delta$, the electron Fermi energy $E_F = E_c = 11$ meV, and the length of the segment without SOI between the two SOI segments $l_1 = 2676$ Å to satisfy $k_0 l_1 = 2\pi$. In the zero temperature panel, we see a periodic beating pattern similar to that of the one-segment wire plotted in Fig. 6(a), but with a period $l_1 = 2676$ Å half of the one-segment one. The origin of the beating pattern is the difference of the spin-precession frequencies in different subbands. Because $k_0 l_1 = 2\pi$, Eq. (20) reduces to Eq. (19) and the partial conductance $G_1^\pm \sim 1 + \cos(10k_\delta l_2)$ and $G_2^\pm \sim 1 + \cos(6k_\delta l_2)$. We note that the conductance pattern shows a sensitive dependence on the length of segment without SOI. If $l_1 = 2000$ Å is chosen, for example, the numerical result shows that both $G_1^\pm$ and $G_2^\pm$ have a dependence close to $1 + \cos(8k_\delta l_2)$ and the conductance pattern becomes completely different. At finite temperature, as shown in the lower panel where $T=2$K, the output polarization of the electron current and the amplitude of the beating pattern decrease with the length of the structure as pointed out also in Ref. 27. The oscillation amplitude becomes half of the initial value at $l_2 = 8000$ Å so we can estimate that the depolarization length due to the subband mixing in this structure is of the order of micrometer at $T=2$ K.

V. CONCLUSION

We have studied the SOI-interface effect on the ballistic spin transport through quantum wires composed of a series of segments with and without SOI. At low electron density, when the Fermi energy of the electron gas is much lower than the second subband, the total conductance is modulated sinusoidally but the outgoing spin orientation remains the same as that without SOI interfaces. In periodic structures the modulation of the total transmission develops into square gaps when the length of the SOI segments or the electron energy are varied. This feature is similar to that obtained previously in stubbed waveguides[28,29] with constant strength α everywhere and has potential applications in establishing a spin transistor.

At higher density, when two subbands are occupied, the outgoing spin orientation is further modulated due to the SOI-induced subband mixing. For electrons with energy close to the anticrossing one the transmission pattern is approximately periodic as function of the length of the SOI segments if the intrasubband SOI splitting k_α is a rational multiple of the intersubband one k_δ, though generally the two-subband transmission patterns are complex. The reflection resulting from the SOI interfaces can be very significant when several SOI segments exist along the quantum wire separated by non-SOI segments. In this case the transmission and outgoing spin orientation can be sensitive to the length of the non-SOI segments as well as to that of the SOI segments.

Finally, the theoretical treatment presented here can also be used to study quantum spin transport in quantum wires in which the SOI strength varies continuously. To do so one simply has to divide the wire into a series of segments, inside which the SOI strength can be treated approximately as constant, with a different value from segment to segment.

ACKNOWLEDGMENTS

The author thanks Professor P. Vasilopoulos for stimulating discussions and useful suggestions. This work was supported by the Canadian NSERC Grant No. OGP0121756.

*Electronic address: xuefeng@alcor.concordia.ca

[1] J. Luo, H. Munekata, F.F. Fang, and P.J. Stiles, Phys. Rev. B **41**, 7685 (1990); B. Das, D.C. Miller, S. Datta, R. Reifenberger, W.P. Hong, P.K. Bhattacharya, J. Singh, and M. Jaffe, *ibid.* **39**, 1411 (1989).

[2] T. Hassenkam, S. Pedersen, K. Baklanov, A. Kristensen, C.B. Sorensen, P.E. Lindelof, F.G. Pikus, and G.E. Pikus, Phys. Rev. B **55**, 9298 (1997).

[3] J. Nitta, T. Akazaki, H. Takayanagi, and T. Enoki, Phys. Rev. Lett. **78**, 1335 (1997).

[4] G. Engels, J. Lange, Th. Schapers, and H. Luth, Phys. Rev. B **55**, R1958 (1997).

[5] T. Matsuyama, R. Kursten, C. Meissner, and U. Merkt, Phys. Rev. B **61**, 15 588 (2000).

[6] C.-M. Hu, C. Zehnder, Ch. Heyn, and D. Heitmann, Phys. Rev. B **67**, 201302(R) (2003).

[7] A.C.H. Rowe, J. Nehls, R.A. Stradling, and R.S. Ferguson, Phys. Rev. B **63**, 201307 (2001).

[8] R. Fiederling, M. Keim, G. Reuscher, W. Ossau, G. Schmidt, A. Waag, and L.W. Molenkamp, Nature (London) **402**, 787 (1999).

[9] B.T. Jonker, Y.D. Park, B.R. Bennett, H.D. Cheong, G. Kioseoglou, and A. Petrou, Phys. Rev. B **62**, 8180 (2000); V.F. Motsnyi, J. De Boeck, J. Das, W. Van Roy, G. Borghs, E. Goovaerts, and V.I. Safarov, Appl. Phys. Lett. **81**, 265 (2002).

[10] R.M. Potok, J.A. Folk, C.M. Marcus, and V. Umansky, Phys. Rev. Lett. **89**, 266602 (2002).

[11] Y. Ohno, D.K. Young, B. Beschoten, F. Matsukura, H. Ohno, and D.D. Awschalom, Nature (London) **402**, 790 (1999).

[12] J.C. Egues, Phys. Rev. Lett. **80**, 4578 (1998).

[13] F. Mireles and G. Kirczenow, Phys. Rev. B **66**, 214415 (2002).

[14] C.M. Hu and T. Matsuyama, Phys. Rev. Lett. **87**, 066803 (2001); T. Matsuyama, C.-M. Hu, D. Grundler, G. Meier, and U. Merkt, Phys. Rev. B **65**, 155322 (2002).

[15] M.H. Larsen, A.M. Lunde, and K. Flensberg, Phys. Rev. B **66**, 033304 (2002).

[16] G. Schmidt, D. Ferrand, L.W. Molenkamp, A.T. Filip, and B.J. van Wees, Phys. Rev. B **62**, R4790 (2000).

[17] E.I. Rashba, Phys. Rev. B **62**, R16267 (2000); A. Fert and H. Jaffres, *ibid.* **64**, 184420 (2001).

[18] E.I. Rashba, Fiz. Tverd. Tela (Leningrad) **2**, 1224 (1960) [Sov. Phys. Solid State **2**, 1109 (1960)]; G. Dresselhaus, Phys. Rev. **100**, 580 (1955).

[19] S. Datta and B. Das, Appl. Phys. Lett. **56**, 665 (1990).

[20] Y.A. Bychkov and E.I. Rashba, J. Phys. C **17**, 6039 (1984).

[21] A.V. Moroz and C.H.W. Barnes, Phys. Rev. B **61**, R2464 (2000).

[22] E.A. de Andrade e Silva and G.C. La Rocca, Phys. Rev. B **67**, 165318 (2003).

[23] M. Governale and U. Zulicke, Phys. Rev. B **66**, 073311 (2002).

[24] A.V. Moroz, K.V. Samokhin, and C.H.W. Barnes, Phys. Rev. Lett. **84**, 4164 (2000).

[25] J.C. Egues, G. Burkard, and D. Loss, Phys. Rev. Lett. **89**, 176401 (2002).

[26] L.W. Molenkamp, G. Schmidt, and G.E.W. Bauer, Phys. Rev. B **64**, 121202(R) (2001); U. Zulicke and C. Schroll, Phys. Rev. Lett. **88**, 029701 (2002).

[27] F. Mireles and G. Kirczenow, Phys. Rev. B **64**, 024426 (2001).

[28] X.F. Wang, P. Vasilopoulos, and F.M. Peeters, Appl. Phys. Lett. **80**, 1400 (2002); Phys. Rev. B **65**, 165217 (2002).

[29] X.F. Wang and P. Vasilopoulos, Phys. Rev. B **68**, 035305 (2003).

[30] J.C. Egues, G. Burkard, and D. Loss, Appl. Phys. Lett. **82**, 2658 (2003).

[31] X. F. Wang and P. Vasilopoulos (unpublished).